Article

Ultrathin and Electrically Tunable Metamaterial with Nearly Perfect Absorption in Mid-Infrared

Yuexin Zou [1], Jun Cao [2] , Xue Gong [2], Ruijie Qian [2] and Zhenghua An [2,*]

[1] Laboratory of Advanced Materials, Fudan University, Shanghai 200438, China
[2] Department of Physics, Fudan University, Shanghai 200438, China
[*] Correspondence: anzhenghua@fudan.edu.cn; Tel.: +86-021-6564-3290

Abstract: Metamaterials integrated with graphene exhibit tremendous freedom in tailoring their optical properties, particularly in the infrared region, and are desired for a wide range of applications, such as thermal imaging, cloaking, and biosensing. In this article, we numerically and experimentally demonstrate an ultrathin (total thickness $< \lambda_0/15$) and electrically tunable mid-infrared perfect absorber based on metal–insulator–metal (MIM) structured metamaterials. The Q-values of the absorber can be tuned through two rather independent parameters, with geometrical structures of metamaterials tuning radiation loss (Q_r) of the system and the material loss ($\tan\delta$) to further change mainly the intrinsic loss (Q_a). This concise mapping of the structural and material properties to resonant mode loss channels enables a two-stage optimization for real applications: geometrical design before fabrication and then electrical tuning as a post-fabrication and fine adjustment knob. As an example, our device demonstrates an electrical and on-site tuning of ~5 dB change in absorption near the perfect absorption region. Our work provides a general guideline for designing and realizing tunable infrared devices and may expand the applications of perfect absorbers for mid-infrared sensors, absorbers, and detectors in extreme spatial-limited circumstances.

Keywords: metamaterial; perfect absorber; graphene; coupled-mode theory; tunable device

1. Introduction

Metamaterial absorbers are two-dimensional electromagnetic structures absorbing light at the resonance, which have attracted huge attention over the years [1–3]. Many functional absorbers integrated with various metamaterial structures have been reported [4–6], holding potential in a broad range of applications, such as sensors [7], spectroscopy [8], and thermal emitters [9,10]. In particular, a metamaterial perfect absorber (MPA) based on a metal–insulator–metal (MIM) structure has been a hotspot for researchers due to its near unity absorptivity. By optimizing the periodic subwavelength arrays topping the device, with the bottom layer as effective reflector, near unity absorption can be achieved at its resonance. Although different types of perfect absorbers with various metamaterial structures have been widely investigated and analyzed [11–15], the realization of MPA structures typically requires heavy computation and repetitive trial and error experiments to achieve the critical damping condition (i.e., $Q_r = Q_a$, where Q_r and Q_a are quality factors related to radiative loss and intrinsic loss, respectively), because a large amount of geometrical and material parameters are involved and entangled. It is therefore anticipated that the independent tuning of Q_r and Q_a by individual parameters can facilitate the easy design. What's more, absorbers in extreme forms, like ultrathin and compact absorbers, are desirable for scaling down the device size and/or minimizing parasitic effects, such as thermal leak conductance and large heat capacity for bolometric detector arrays [16–20].

With its unique electronic and optical features, graphene has drawn tremendous attention in recent years [21,22]. Graphene, with a single atomic layer thickness of only 0.33 nm, is by now the

thinnest two-dimensional material and exhibits the remarkable property of changing its conductivity through electrical modulation [23]. Graphene has been reported to be applicable for modulators over a large wavelength region, ranging from near-infrared to far-infrared frequencies [24–27]. As a result, graphene integrated into metamaterials provides tremendous freedom in tailoring their optical properties. The reported works, however, typically utilized complicated device structures, such as ion-gel gating, to realize electrical modulation [28] and sophisticated interplay between graphene and background absorption remains elusive. It is therefore desirable to design more compact metamaterials with built-in tunability.

In this article, we demonstrate an ultrathin and electrically tunable graphene MIM metamaterial perfect absorber working at the mid-infrared region, with a total thickness of ~270 nm (thickness < $\lambda_0/15$). The MIM tri-layer structure forms an agile platform to engineer the infrared optical properties of the structure. The bottom metal layer of the MIM structure provides two-fold functions: a mirror to form resonant cavity and an effective gate to adjust the Fermi level in the graphene layer, and hence the absorption. This tunable absorption provides a compact, flexible, and post-fabrication fine adjustment freedom to the hybrid metamaterials.

2. Materials and Methods

The metamaterial absorbers were fabricated on a Si_3N_4 membrane with supporting Si frame, as schematically illustrated in Figure 1a. The thickness of the Si_3N_4 membrane was 200 nm. A series of nano-fabrication processes were performed on the membrane. The reflecting layer underneath the membrane, which was also used as the back-gate of the absorber, was prepared with 5 nm Cr and 30 nm Au by electron beam evaporation. Graphene on top of Si_3N_4 was grown using the chemical vapor deposition (CVD) method and subsequently transferred onto the membrane. Source and drain contacts, grown with 5 nm Cr and 50 nm Au, were then fabricated onto the graphene by photolithography procedures. Standard electron-beam lithography and lift-off processes were finally used to pattern the cross-shaped Au metamaterial arrays (5 nm Cr/30 nm Au), whose scanning electron microscope (SEM) image is shown in Figure 1b. For each absorber, the total patterned area was about 50 μm × 50 μm. The period (P) of each square unit cell in these arrays was 2.3 μm, while the arm width (W) and arm length (L) of the cross-shaped microstructures were to be optimized. All of the following optical and electrical experiments were carried out at room temperature.

The reflectance spectra of our absorbers are shown in Figure 1c, with the back-gate voltage fixed at 0 V. Considering the transmittance of the device with a reflecting layer underneath the Si_3N_4 membrane was nearly 0, the absorption (A) of our device is closely related to the reflectance (R). Their relationship can be written as A = 1 − R. From Figure 1c, the reflectance of the absorber without a metasurface was nearly constant and equal to 1, indicating that the absorber reflected almost all the mid-infrared light without noticeable absorption. For those with different patterns, different modes of localized plasmon induced by metamaterial arrays can resonate with light of a specific wavelength. With the help of the reflecting layer, the light trapped in the Si_3N_4 membrane will finally contribute to the absorption of the device. As a result, mid-infrared light is largely absorbed at the resonant wavelength. The absorber with parameters of L = 1.25 μm and W = 0.3 μm exhibited the best performance, with reflectance < 0.03, or absorptance > 0.963, at the frequency of 2013 cm^{-1}. The reflectance of the device was mainly influenced by the length and width of the arm. More systematic studies indicate that a longer arm length results in a red-shift of its resonant frequency, while the arm width affects the depth of reflectance [29]. These patterns can generate different dips in reflectance at its resonance frequency. Figure 1d depicts numerical results based on the Finite-Difference Time-Domain (FDTD) method. The parameters of the MIM structure in the simulation were nearly identical to our experiments. The metals in the simulation were based on the Drude model. The plasma frequency for Au was set to be $\omega_p = 1.365 \times 10^{16}$ rad/s and the collision frequency was $\gamma = 5.78 \times 10^{13}$ Hz. The relative permittivity for the semiconductor layer (Si_3N_4) was chosen to be 3 [30]. The perfect matched layer was introduced as the boundary condition in our system. The simulation results are reasonably consistent

with our experimental results, except that the absorption peaks are wider and the absorption rates are lower in the experiments than in the simulation. The discrepancy in peak width may have arisen from the imperfection of the sample fabrication, such as variations in period and length, which were not considered in the simulation. However, it is certain that the MIM structures offers an important and effective approach to design a cavity-like absorber, which can efficiently harvest mid-infrared photons for real applications.
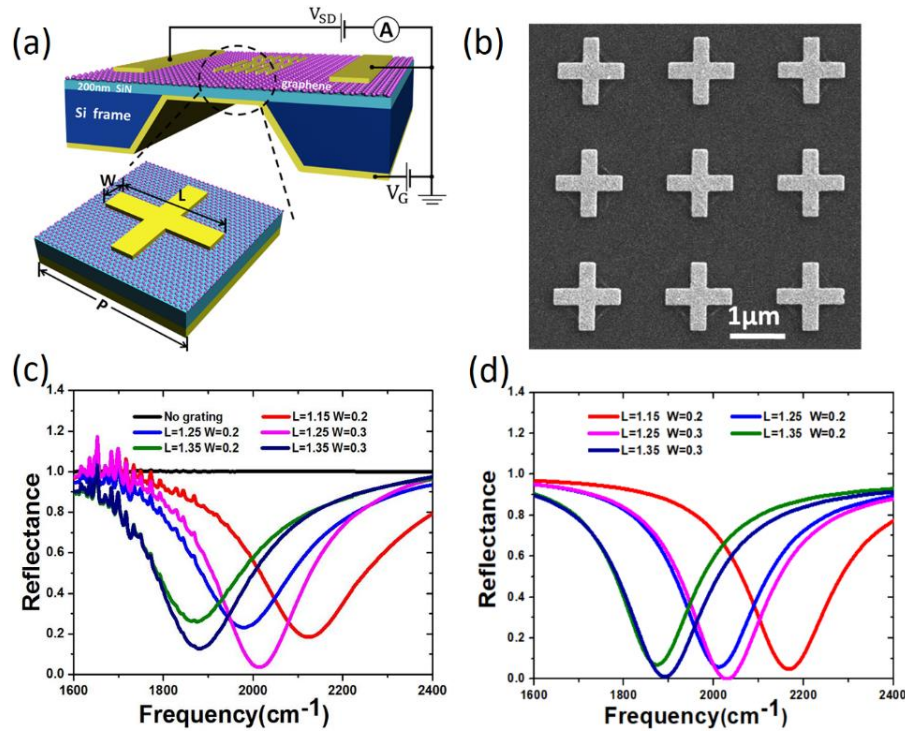
Figure 1. (**a**) The schematic of the graphene metamaterial perfect absorber and the unit cell of the metamaterial arrays. The tunable reflectance can be achieved by back-gating of graphene between the Si$_3$N$_4$ membrane and the metasurface. (**b**) The SEM image of the metamaterial structure topping the absorber, with L = 1.25 μm and W = 0.3 μm. (**c**) Reflectance spectra for the absorbers in (**a**) with different metamaterial structures. (**d**) Simulated results for the same structures in (**c**).

3. Results and Discussion

According to coupled-mode theory (CMT) [28,29,31,32], the optical properties of the MIM structures are determined essentially by two competing loss channels, namely, the radiation loss of the resonance cavity and intrinsic loss due to material absorption. The tunable property of the MIM structure is therefore realizable by changing either of these two channels. From CMT theory, the reflection coefficient (r) of our system can be written as [29],

$$r(\omega) = -1 + \frac{2/\tau_r}{-i(\omega - \omega_0) + 1/\tau_r + 1/\tau_a},$$ (1)

where and $1/\tau_a$ are the decay rates of radiation and absorption, respectively. Furthermore, the radiative and absorptive quality factors (Q-value) of the system are defined as $Q_r = \omega_0\tau_r/2$ and $Q_a = \omega_0\tau_a/2$, which determine the physical properties of the system. From Equation (1), $r(\omega_0) = \frac{Q_a/Q_r - 1}{Q_a/Q_r + 1}$ when frequency is at its resonance ($\omega = \omega_0$), which shows that Q_a/Q_r is the physical quantity to decide the minimum reflection or maximum absorption. Based on Equation (1) and the definitions of Q_a and Q_r we mentioned above, Q_a and Q_r of the system with specific structural parameters can be obtained through numerical fitting of our simulation or experimental results [29]. Figure 2a depicts the phase

diagram of Q_a/Q_r as a function of the geometrical parameter W and the material loss tanδ. tanδ defines the dielectric loss angular tangent of the system, which can indicate the inherent dissipation (such as heat) of electromagnetic energy in the dielectric layer [33]. When $Q_r > Q_a$, the resonator is overdamped and the variation of phase only occupies a small range, less than 180°. The solid line shows the perfect absorption condition with $Q_r = Q_a$. Interestingly, this line shows a simple and approximately linear dependence in the region with small W ($\leq$0.6 µm) and tanδ ($\leq$0.08) This implies that the loss channel of the resonant mode may depend on specific parameters, W or tanδ. In Figure 2b,c, Q_r and Q_a are displayed as functions of W or tanδ when the other one is fixed. It is obvious that Q_r is affected mainly by W ($\leq$0.6 µm), while Q_a is affected by tanδ. This appears to be physically reasonable, since the non-radiative loss leads to material absorption and therefore depends on the imaginary part of its dielectric permittivity, while the radiation loss relies on the dipole oscillation strength of the resonant mode and hence increases with W. When W > 0.6 µm, the field distribution becomes dramatically different from the case with small W, which prevents the radiative loss rate from further increase.
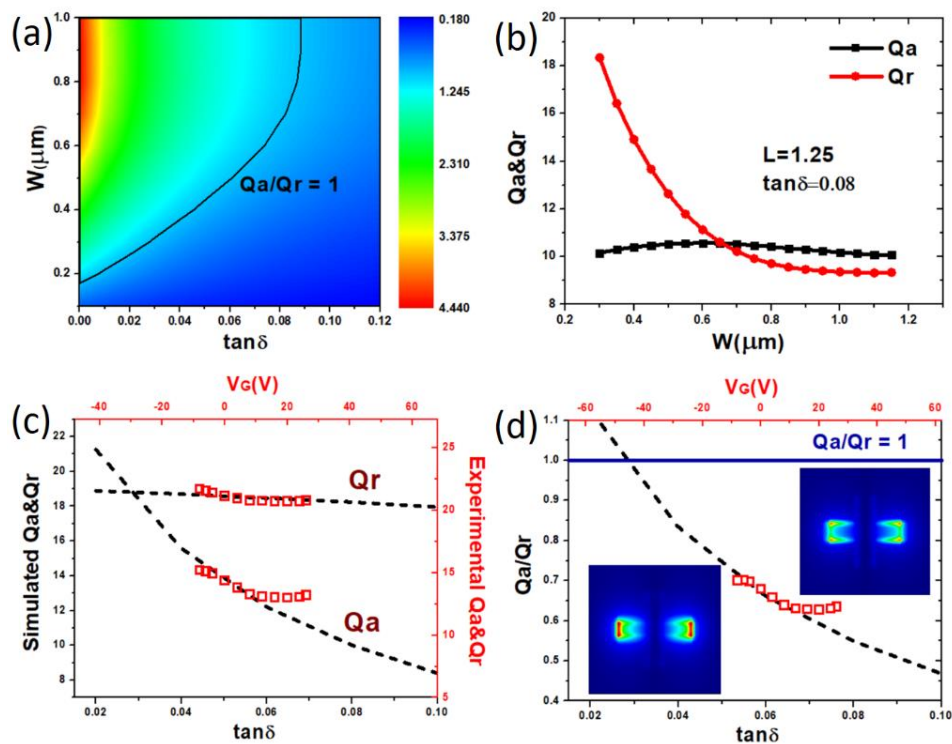

Figure 2. (**a**) The ratio between Q_a and Q_r, with different W and tanδ. (**b**) Q_a and Q_r change when L = 1.25 µm and tanδ = 0.08. (**c**) Black dashed lines indicate the quality factor (Q_a and Q_r) of the simulated results with fixed W, while red square dots show the experimentally tunable regime of graphene modulated by electricity. (**d**) Q_a/Q_r of the simulated and experimental results. 2D polarization images depict $|E_Z|$ distribution at $V_G = -8$ V and $V_G = 26$ V.

The above scenario provides useful hints for the realization of tunable infrared devices with nearly perfect absorption. Experimentally, we examined the tuning performance through back-gating in our compact MIM structure with fixed geometrical parameters (L = 1.25 µm and W = 0.3 µm). The Raman spectra of the graphene we used are shown in Figure 3a. The inset figure in Figure 3a shows the Raman spectrum of the graphene after being integrated into our device using an excitation laser of λ = 633 nm. We can clearly see that the intrinsic G peak and 2D peak of graphene are around 1580 cm^{-1} and 2680 cm^{-1}, which are consistent with precious reports [34], despite the series of nano-fabrication processes. The source-drain current (I_{SD}) in graphene is modulated by back-gate bias (V_G), which is shown in Figure 3b. When the source–drain current reaches its lowest level, namely $V_G = V_F$, which is at around 17 V, the Fermi level matches the Dirac point. As the back-gate voltage increases,

the source–drain current curve shows an obvious kink shape, indicating that the concentration of carriers in graphene is varying due to the change of Fermi energy level (V_F). When $V_G < V_F$, the carriers transported in graphene are hole-dominated, and when $V_G < V_F$, transport in graphene is electron-dominated.
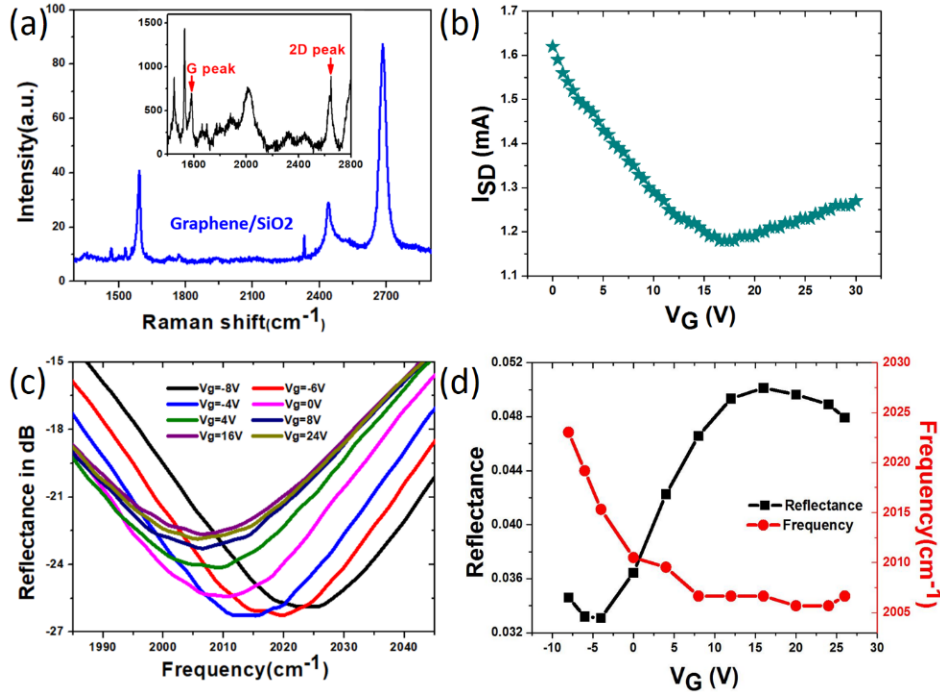
Figure 3. (**a**) Raman spectra of the graphene we used coating on SiO_2 substrate and the graphene integrated in the absorber with cross arrays of L = 1.25 μm and W = 0.3 μm (inset figure). The wavelength of the applied laser is 633 nm. (**b**) The source–drain current is controlled by back-gating. Dirac point is achieved at around the bias of 17 V. The reflectance spectra of the absorbers with different cross-shaped metamaterials. (**c**) Modulation of reflectance achieved by back-gating of graphene with cross-shaped metamaterial of L = 1.25 μm and W = 0.3 μm. (**d**) The change in reflectance and frequencies at different back-gate bias.

Figure 3c shows the reflection spectra at different back-gate voltages. It can be seen that the reflection spectra can be tuned continuously by the gate bias, and the change of $r(\omega_0)$ due to back-gating can reach about 5 dB (dip-to-dip). The minimum reflectance, $r(\omega_0)$, at different biases is depicted as black squares in Figure 3d. From Figure 3d, the largest reflection value at resonant dip is near the Dirac point ($V_G \sim 17$ V) and, with increasing the carrier density (no matter electron or hole), the reflection value decreases, which indicates additional absorption. In the meantime, with decreasing V_G, the resonant frequency increases slightly ($\sim$1%), which may be ascribed to a smaller effective mode volume. The rather limited tunability of the present device is associated with the quality of the graphene layer, which consisted of impurities and defects due to CVD growth and device fabrication processing. The tunability can be further improved with better sample quality or using BN/graphene/BN sandwiched structures.

To reveal the physical insights behind the demonstrated tunability, we followed CMT and numerically fit the experimental data with equation 1 to extract Q_r and Q_a values. As the reflectances ($R = |r(\omega)|^2$) of the device under different bias are known, Q_r and Q_a of the system can be easily obtained by numerical fitting based on Equation (1). The results are shown by red hollow squares in Figure 2c and it can be seen that the extracted Q_r and Q_a agree reasonably with the simulation data. This agreement validates the simplified model to treat graphene as an effective layer with tunable absorption. The apparent deviation in the region of $V_G > 17$ V is attributable to the fact that carriers

are inverted into electron type, and that the carrier density shows a non-monotonous dependency upon V_G. In the region of $V_G < 17$ V, Q_r appears to be almost independent of back-gating, while Q_a can be considerably modulated by back-gate biasing. The Q_a/Q_r value extracted from experimental data is also displayed in Figure 2d, and a similar agreement can be clearly identified. 2D images in the inset of Figure 2d show the modular z-component of the electric field ($|E_Z|$) of a unit cell at $V_G = -8$ V and $V_G = 26$ V. As V_G decreases, the difference between Q_r and Q_a also decreases. Accordingly, the electrical field around the cross increases, which leads to a condition closer to perfect absorption ($Q_a/Q_r = 1$). In our present work, although the Q_a/Q_r change covered only a limited interval along the dashed line and perfect absorption ($Q_a/Q_r = 1$) was not yet reached, it is evident that electrical tuning of graphene Fermi level by back-gating is effective for modulating the optical property of the hybrid metamaterial structure. In addition, it is expected that electrical tuning at a different geometrical parameter W (and therefore different Q_r) will lead to a different tunable range, and the same electrical gating at a larger W will lead to possibly perfect absorption, as indicated by the phase diagram in Figure 2a.

4. Conclusions

In summary, we studied an ultrathin ($< \lambda_0/15$) and electrically tunable graphene metamaterial perfect absorber working at the mid-infrared region. The Q-values of the absorber can be tuned through rather independent parameters, namely, radiation loss (Q_r), mainly modulated by W, and intrinsic loss (Q_a) by the graphene with tunable absorption through back-gating. Our work suggests that near-independent Q-tuning could be realized by integrating graphene into metamaterial absorbing systems, which may facilitate the devising and experimental process of finding critical damping. Our work also provides new thinking for designing and realizing tunable infrared devices, and may be valuable for wider applications of perfect absorbers in mid-infrared sensors, absorbers, and detectors.

Author Contributions: Y.Z. conceived and performed the experiments, analyzed the data, and wrote the paper. Z.A. provided the experimental materials and laboratory equipment and directed the research. J.C., X.G., and R.Q. contributed to the discussion and interpretation of the results.

Conflicts of Interest: The authors declare no conflicts of interest.

References

1. Liu, X.; Starr, T.; Starr, A.F.; Padilla, W.J. Infrared Spatial and Frequency Selective Metamaterial with Near-Unity Absorbance. *Phys. Rev. Lett.* **2010**, *104*, 207403. [CrossRef]
2. Ogawa, S.; Kimata, M. Metal-Insulator-Metal-Based Plasmonic Metamaterial Absorbers at Visible and Infrared Wavelengths: A Review. *Materials* **2018**, *11*, 458. [CrossRef] [PubMed]
3. Kildishev, A.V.; Boltasseva, A.; Shalaev, V.M. Planar Photonics with Metasurfaces. *Science* **2013**, *339*, 1232009. [CrossRef]
4. Chen, H.; Padilla, W.; Zide, J.; Gossard, A.; Taylor, A.; Averitt, R. Active terahertz metamaterial devices. *Nature* **2006**, *444*, 597–600. [CrossRef] [PubMed]
5. Zhu, H.; Yi, F.; Cubukcu, E. Plasmonic metamaterial absorber for broadband manipulation of mechanical resonances. *Nat. Photonics* **2016**, *10*, 709–714. [CrossRef]
6. Luo, L.; Chatzakis, I.; Wang, J.; Niesler, F.; Wegener, M.; Koschny, T.; Souloulis, C. Broadband terahertz generation from metamaterials. *Nat. Commun.* **2014**, *5*, 3055. [CrossRef] [PubMed]
7. Ogawa, S.; Takagawa, Y.; Kimata, M. Polarization-selective uncooled infrared sensor using a one dimensional plasmonic grating absorber. *Proc. SPIE Infrared Technol. Appl. XLI* **2015**, *9451*, 94511K. [CrossRef]
8. Chen, K.; Adato, R.; Altug, H. Dual-Band Perfect Absorber for Multispectral Plasmon-Enhanced Infrared Spectroscopy. *ACS Nano* **2012**, *6*, 7998–8006. [CrossRef] [PubMed]

9. Liu, X.; Tyler, T.; Starr, T.; Starr, A.F.; Jokerst, N.M.; Padilla, W.J. Taming the Blackbody with Infrared Metamaterials as Selective Thermal Emitters. *Phys. Rev. Lett.* **2011**, *107*, 045901. [CrossRef]

10. Argyropoulos, C.; Le, K.; Mattiucci, N.; D'Aguanno, G.; Alu, A. Broadband absorbers and selective emitters based on plasmonic Brewster metasurfaces. *Phys. Rev. B* **2013**, *87*, 205112. [CrossRef]

11. Zheludev, N.I.; Kivshar, Y.S. From metamaterials to metadevices. *Nat. Mater.* **2012**, *11*, 917–924. [CrossRef] [PubMed]

12. Bowen, P.T.; Baron, A.; Smith, D.R. Theory of patch-antenna metamaterial perfect absorbers. *Phys. Rev. A* **2016**, *93*, 063849. [CrossRef]

13. Ding, F.; Yang, Y.; Deshpande, R.A.; Bozhevolnyi, S.I. A review of gap-surface plasmon metasurfaces: Fundamentals and applications. *Nanophotonics* **2018**, *7*, 1129–1156. [CrossRef]

14. Cui, Y.; He, Y.; Jin, Y.; Ding, F.; Yang, L.; Ye, Y.; Zhong, S.; Lin, Y.; He, S. Plasmonic and metamaterial structures as electromagnetic absorbers. *Laser Photonics Rev.* **2014**, *8*, 495–520. [CrossRef]

15. Alaee, R.; Farhat, M.; Rockstuhl, C.; Lederer, F. A perfect absorber made of graphene micro-ribbon metamaterial. *Opt. Express* **2012**, *20*, 28017–28024. [CrossRef] [PubMed]

16. Yahiaoui, R.; Tan, S.; Cong, L.; Singh, R.; Yan, F.; Zhang, W. Multispectral terahertz sensing with highly flexible ultrathin metamaterial absorber. *J. Appl. Phys.* **2015**, *118*, 083103. [CrossRef]

17. Deng, H.; Li, Z.; Stan, L.; Rosenmann, D.; Czaplewski, D.; Cao, J.; Yang, X. Multispectral terahertz sensing with highly flexible ultrathin metamaterial absorber. *Opt. Lett.* **2015**, *40*, 2592. [CrossRef] [PubMed]

18. Xiong, H.; Wu, Y.; Dong, J.; Tang, M.; Jiang, Y.; Zeng, X. Ultra-thin and broadband tunable metamaterial graphene absorber. *Opt. Express* **2018**, *26*, 1681–1688. [CrossRef]

19. Huang, L.; Chowdhury, D.R.; Ramani, S.; Reiten, M.T.; Luo, S.; Azad, A.K.; Taylor, A.J.; Chen, H. A Novel Approach to Further Decrease the Thickness of Ultrathin Perfect Metamaterial Absorbers. In Proceedings of the IEEE Conference on 2012 International Workshop on Metamaterials (Meta), Nanjing, China, 8–10 October 2012; pp. 1–3. Available online: https://ieeexplore.ieee.org/document/6464921/ (accessed on 24 July 2018).

20. Butun, S.; Aydin, K. Structurally tunable resonant absorption bands in ultrathin broadband plasmonic absorbers. *Opt. Express* **2014**, *22*, 19457–19468. [CrossRef]

21. Koppens, F.H.L.; Mueller, T.; Anouris, P.; Ferrari, A.C.; Vitiello, M.S.; Polini, M. Photodetectors based on graphene, other two-dimensional materials and hybrid systems. *Nat. Nanotec.* **2014**, *9*, 780–793. [CrossRef]

22. Bonaccorso, F.; Sun, Z.; Hasan, T.; Ferrari, A. Graphene Photonics and Optoelectronics. *Nat. Photonics* **2010**, *4*, 611–622. [CrossRef]

23. Nair, R.R.; Blake, P.; Grigorenko, A.N.; Novoselov, K.S.; Booth, T.J.; Stauber, T.; Peres, N.M.R.; Geim, A.K. Fine Structure Constant Defines Visual Transparency of Graphene. *Science* **2008**, *320*, 1308. [CrossRef]

24. Zhu, W.; Rukhlenko, I.D.; Premaratne, M. Graphene metamaterial for optical reflection modulation. *Appl. Phys. Lett.* **2013**, *102*, 241914. [CrossRef]

25. Lee, S.H.; Choi, M.; Kim, T.-T.; Lee, S.; Liu, M.; Yin, X.; Choi, H.K.; Lee, S.S.; Choi, C.-G.; Choi, S.-Y.; et al. Switching terahertz waves with gate-controlled active graphene metamaterials. *Nat. Mater.* **2012**, *11*, 936–941. [CrossRef] [PubMed]

26. Vasic, B.; Gajic, R. Graphene induced spectral tuning of metamaterial absorbers at mid-infrared frequencies. *Appl. Phys. Lett.* **2013**, *103*, 261111. [CrossRef]

27. Li, Z.; Yu, N. Modulation of mid-infrared light using graphene-metal plasmonic antennas. *Appl. Phys. Lett.* **2013**, *102*, 131108. [CrossRef]

28. Miao, Z.; Wu, Q.; Li, X.; He, Q.; Ding, K.; An, Z.; Zhang, Y.; Zhou, L. Widely Tunable Terahertz Phase Modulation with Gate-Controlled Graphene Metasurfaces. *Phys. Rev. X* **2015**, *5*, 041027. [CrossRef]

29. Yu, H.; Zhao, Z.; Qian, Q.; Xu, J.; Gou, P.; Zou, Y.; Cao, J.; Yang, L.; Qian, J.; An, Z. Metamaterial perfect absorbers with solid and inverse periodic cross structures for optoelectronic applications. *Opt. Express* **2017**, *25*, 8288–8295. [CrossRef]

30. Luke, K.; Okawachi, Y.; Lamont, M.R.E.; Gaeta, A.L.; Lipson, M. Broadband mid-infrared frequency comb generation in a Si_3N_4 microresonator. *Opt. Lett.* **2015**, *40*, 4823–4826. [CrossRef]

31. Haus, H.A.; Huang, W. Coupled-Mode Theory. *IEEE* **1991**, *79*, 1505–1508. [CrossRef]

32. Qu, C.; Ma, S.; Hao, J.; Qiu, M.; Li, X.; Xiao, S.; Miao, Z.; Dai, N.; He, Q.; Sun, S.; et al. Tailor the Functionalities of Metasurfaces Based on a Complete Phase Diagram. *Phys. Rev. Lett.* **2015**, *115*, 235503. [CrossRef] [PubMed]

33. Chen, L.F.; Ong, C.K.; Neo, C.P.; Varadan, V.V.; Varadan, V.K. *Microwave Electronics: Measurement and Materials Characterization*, 1st ed.; Wiley: Chichester, UK, 2004; pp. 12–14.

34. Malard, L.M.; Pimenta, M.A.; Dresselhaus, G.; Dresselhaus, M.S. Raman spectroscopy in graphene. *Phys. Rep.* **2009**, *473*, 51–87. [CrossRef]